$NaRb_3B_6O_9(OH)_3(HCO_3)$: A Borate-bicarbonate Nonlinear Optical Material.

Fenghua Ding,[†] *Weilong Zhang,*[‖] *Matthew Nisbet,*[†] *Weiguo Zhang,*[‡] *P. Shiv Halasyamani,*[‡] *Zhihua Yang,*[§] *Shilie Pan,*[§] *and Kenneth R. Poeppelmeier*[*,†]

[†]Department of Chemistry, Northwestern University, Evanston, Illinois 60208, United States

[‡] Department of Chemistry, University of Houston, Houston, Texas 77204, United States.

[§] Key Laboratory of Functional Materials and Devices for Special Environments and Key Laboratory of Electronic Information Materials and Devices, Xinjiang Technical Institute of Physics & Chemistry, Chinese Academy of Sciences, 40-1 South Beijing Road, Urumqi 830011, China

[‖] College of Electronics and Information Science, Fujian Jiangxia University, Fuzhou 350108, P. R. China

ABSTRACT: A non-centrosymmetric mixed alkaline borate-bicarbonate, $NaRb_3B_6O_9(OH)_3(HCO_3)$, was synthesized and characterized. The compound crystallizes in space group $P2_1$ (No. 4) with cell parameters of a=8.988(3) Å, b=8.889(2) Å, c=10.068(4) Å and β=114.6(4)°. The structure features a combination of chains of boron-oxygen $[B_6O_9(OH)_3]^{3-}$ groups and isolated HCO_3^- groups, with charge compensation provided by Rb^+ and Na^+ cations. The UV-Vis-NIR absorption spectrum indicated a transparence of about 40% at 200 nm. The IR spectrum confirmed the coordination environments of anionic groups, and the compound is thermally stable up to ~320 °C. Additionally, first-principles calculations were performed in order to gain insight into the role of boron-oxygen and HCO_3^- groups with respect to the band structure and NLO properties. The bicarbonate (HCO_3^-) anion has enhanced hyperpolarizability relative to the carbonate (CO_3^{2-}) anion.

Introduction

Deep ultraviolet (DUV) nonlinear optical (NLO) materials have played an important role in laser science and photonic technology.[1, 2] The first NLO borate crystal described for DUV generation was $KB_5O_8 \cdot 4H_2O$ (KB5).[3] Sixth harmonic generation, i.e. 1064nm / 6 = 177.3nm, of the Nd:YAG laser has been achieved in KB5 by mixing the fundamental and the fifth-harmonic radiation. Although the absorption edge is at 165 nm and the phase matching range of the crystal is down to 200 nm, the output power is unfortunately low attributable to the small nonlinear optical effect of the crystal.[4, 5] Another DUV NLO material, $KBe_2BO_3F_2$ (KBBF) has successfully generated coherent radiation at 177.3 nm by direct second-harmonic generation using a CaF_2 prism coupler.[6-8] However, KBBF suffers from two serious drawbacks (i) toxic BeO is required in the synthesis and (ii) single crystals have a layered growth tendency. With the latter, large single crystals of KBBF are difficult to grow, that greatly limits its wide application. Exploring new DUV NLO materials is still very active because of the absence of a commercial crystal for the DUV region.

Considering the non-centrosymmetric (NCS) structural requirement for NLO crystals, acentric coordination environments of anions are considered, such as rigid tetrahedral groups (e.g., PO_4^{3-}, PO_3F^{2-})[9] and π-conjugated planar groups (e.g., BO_3^{3-}, CO_3^{2-}, NO_3^- and $C_3N_3O_3^{3-}$)[10]. Moreover, with respect to structure-property relationships between the NLO effects and the compounds crystal structure, it is widely accepted that the planar BO_3 groups contribute a relatively large microscopic second-order susceptibility and exhibit moderate birefringence,[11] both of which are desirable for DUV laser generation. Previously many new potential DUV NLO materials based on BO_3 groups, such as borate fluorides ($BaMBO_3F$ (M=Mg, Zn), $A_3B_3Li_2Al_4B_6O_{20}F$ (A=alkali metal; B=alkaline-earth metal),[12-14] $Rb_3Al_3B_3O_{10}F$,[15] $Ba_4B_{11}O_{20}F$[16]; fluorooxoborates ($SnB_2O_3F_2$,[17] $Li_2B_3O_4F_3$, $Li_2B_6O_9F_2$,[18] $NH_4B_4O_6F$,[19] and CsB_4O_6F[20]) have been reported. Analogous to the BO_3 groups, the CO_3 groups possess a similar planar triangle geometry with a π-conjugated molecular orbital. Several carbonate fluorides have been reported to be potential DUV NLO materials, such as $KMgCO_3F$,[21] $RbMgCO_3F$,[22] $ABCO_3F$ (A=K, Rb, Cs; B=Sr, Ca),[23, 24] $AAlCO_3F_2$ (A=alkali metal),[24] $Na_8Lu_2(CO_3)_6F_2$ and $Na_3Lu(CO_3)_2F_2$.[25]

Meanwhile, the incorporation of BO_3 and CO_3 has been proposed in one acentric structure.[26, 27] Twenty-five compounds in the mixed borate and carbonate family have been

reported, ten of which are minerals and fifteen of which are synthetic according to the Inorganic Crystal Structure Database, PDF-4+ and recent publications (Table S1).[26] $Pb_7O(OH)_3(CO_3)_3(BO_3)$[28] was the first reported synthetic borate carbonate with NLO capabilities. Recently, several mixed borate and carbonate halides have been also discovered.[26] However, the absorption edges of these NCS compounds all exceed 200 nm that indicates DUV NLO generation is not possible. The wide transparency range requirement (<200 nm for DUV crystals) narrows the choice of elements to alkali and alkaline-earth metals as host of cations without *d-d* or *f-f* transitions. Two barium borate carbonates, $Ba_3[B_6O_{10}(OH)_2](CO_3)$ and $Ba_6[B_{12}O_{21}(OH)_2](CO_3)_2$, were synthesized by the high-temperature, high-pressure hydrothermal method (460 °C and 600 bar).[27] Another barium borate carbonate chloride, $Ba_2(BO_3)_{1-x}(CO_3)_xCl_{1+x}$, ($0<x<0.5$) was obtained by high temperature method,[29] while two potassium borate carbonate halide, $K_9[B_4O_5(OH)_4]_3(CO_3)X\cdot 7H_2O$ (X = Cl, Br), was synthesized by hydrothermal method.[30]

We report the first synthetic borate-bicarbonate NLO compound, $NaRb_3B_6O_9(OH)_3(HCO_3)$ (SRBOC). A single crystal of the compound was grown by a facile solvothermal method. The structure was discussed and related optical properties were characterized. Band structure of the compound was calculated and optical properties, including polarizability anisotropy and first order hyperpolarizability of HCO_3^-, CO_3^{2-}, and BO_3^{3-} group were compared through theoretical calculations.

Experimental Section

Preparation of $NaRb_3B_6O_9(OH)_3(HCO_3)$

Boric acid (H_3BO_3, 99.0%), rubidium carbonate (Rb_2CO_3, 99.9%), sodium hydroxide (NaOH, 99.0%), and ethyl alcohol (C_2H_6O, Pure 200 proof) were used as received from Sigma-Aldrich. Deionized water was used during the all experiments.

Single crystals of $NaRb_3B_6O_9(OH)_3(HCO_3)$ were synthesized by a solvothermal method. 0.69 g Rb_2CO_3 (3.00 mmol), 0.74 g H_3BO_3 (12.00 mmol), 0.08 g NaOH (2.00 mmol), 0.50 ml ethyl alcohol and 0.16 ml deionized water were added to a Teflon pouch that was sealed and placed into a 125 mL Parr autoclave. The autoclave was backfilled with 50 mL ethyl alcohol. The autoclave was heated to 220 °C, held at this temperature for 48 h, and cooled to room temperature at a rate of 0.1 °C/ min. The crystals were recovered in ~90% yield based on Rb

after vacuum filtration. The photo of single crystal can be found in Figure S1. The final pH value of the solution was 8.45. Single solvent systems of only water or ethanol failed to produce the title compound, thus the necessity of the mixed solvent system (water and ethanol) used in our case can be explained as follows. Water and ethanol are miscible due to their intermolecular hydrogen bonding interactions. However, as electrolytes (in this case H_3BO_3, NaOH and Rb_2CO_3) are added to the system, the solvation of the electrolytes leaves water unavailable to form hydrogen bonds with ethanol, which decreases the solubility of ethanol. This salting-out effect increases the concentration of the solute in the water. Additionally, the ethanol increases the pressure in the reaction vessel at high temperature.

Instruments and Measurements

Powder XRD measurements were performed at room temperature on a Rigaku Ultima diffractometer with graphite monochromatized Cu Kα (λ = 1.5418 Å) radiation. The measured powder XRD patterns of $NaRb_3B_6O_9(OH)_3(HCO_3)$ were in agreement with the simulated patterns from single crystal X-ray diffraction studies (Figure S2).

The Fourier transform infrared spectroscopy (FTIR) spectra in the 600~4000 cm^{-1} range were recorded on a Bruker 37 Tensor FTIR spectrometer at room temperature.

UV-vis diffuse reflectance spectra were collected with a UV-3600 SHIMADZU UV-vis-NIR spectrophotometer over the spectral range of 200~1000 nm at room temperature. Barium sulfate ($BaSO_4$) was used as a standard sample for the baseline correction. The sample was thoroughly mixed with $BaSO_4$, and this mixture was used for UV-vis measurements. Reflectance spectra were converted to absorbance using the Kubelka-Munk equation.[31, 32]

The thermogravimetric analysis (TGA) and differential thermal analysis (DTA) was carried out with a NETZSCH-Proteus-61 analyzer instrument. Crystal samples were added into an aluminum crucible and heated from room temperature to 600 °C at a rate of 10 K/min and then cooled to room temperature at same rate under flowing Helium with flow rate of 25 ml/min.

The SHG measurements of polycrystalline samples were performed with a Nd: YAG (λ = 1064 nm) as the incident light source. Samples of compounds were ground and sieved into seven distinct size ranges for the test. Ground SiO_2 powder were used as a reference and sieved into the same size ranges. The intensities of the frequency-doubled output emitted from the samples were detected by a photomultiplier tube.

Single-Crystal Structure Determination

Colorless and transparent block crystal (Figure S1) with dimensions of 0.112 mm × 0.068 mm × 0.044 mm for $NaRb_3B_6O_9(OH)_3(HCO_3)$ was chosen for structure determination. Single crystal XRD data were obtained at 100 K with a Rigaku Oxford XtaLAB Synergy-DW diffractometer with monochromated Mo *K*α radiation (λ= 0.7107 Å). The crystal-to-detector distances were set as 50 mm. The CrysAlisPro software was used for data reduction and integration.[33] The structures were established by direct method and refined through full-matrix least-squares fitting on F^2 using OLEX2.[34] All atoms were refined using full matrix least-squares techniques, and final least-squares refinement was on F_o^2 with data having $F_o^2 \geq 2\sigma (F_o^2)$. Numerical absorption corrections were carried out using the SCALE program for area detector. The structures were solved with the use of Shel-XT to determine the atomic coordinates of the cations. The structures were examined for possible missing symmetry elements with PLATON and no additional symmetry was found.[35] Other crystallographic data are reported in the CIF.

Calculation details

Optical properties were calculated by first principles calculations based on density-functional theory in the CASTEP package.[36, 37] The functionals developed by Perdew-Burke-Ernzerhof (PBE) in generalized gradient approximation (GGA) form were used to describe the exchange-correlation energy[38]. Under the norm-conserving pseudopotential (NCP),[39] the following orbital electrons were treated as valence electrons: Na $2s^2$ $2p^6$ $3s^1$, Rb $4s^2$ $4p^6$ $5s^1$, B $2s^2$ $2p^1$, C $2s^2$ $2p^2$, O $2s^2$ $2p^4$, H $1s^1$. A kinetic energy cutoff of 830 eV is chosen with 2×2×2 Monkhorst-Pack k-point meshes in the Brillouin zone. The scissors operator correction is adopted to calculated nonlinear optical properties.

The so-called length-gauge formalism derived by Aversa and Sipe[40] was adopted. At a zero frequency, the static second-order nonlinear susceptibilities can be ascribed to Virtual-Hole (VH), Virtual-Electron (VE) processes[41, 42]:

$$\chi^{(2)}_{\alpha\beta\gamma} = \chi^{(2)}_{\alpha\beta\gamma}(\mathrm{VE}) + \chi^{(2)}_{\alpha\beta\gamma}(\mathrm{VH})$$

The formulas for calculating the contribution from VE and VH processes are as follows:

$$\chi^{(2)}_{\alpha\beta\gamma}(\mathrm{VE}) = \frac{e^3}{2\hbar^2 m^3}\sum_{vcc'}\int \frac{d^3k}{4\pi^3} P(\alpha\beta\gamma) Im[P^{\alpha}_{vc} P^{\beta}_{cc'} P^{\gamma}_{c'v}] \left(\frac{1}{\omega^3_{cv}\omega^2_{vc'}} + \frac{2}{\omega^4_{vc}\omega_{c'v}}\right)$$

$$\chi^{(2)}_{\alpha\beta\gamma}(\mathrm{VH}) = \frac{e^3}{2\hbar^2 m^3}\sum_{vv'c}\int \frac{d^3k}{4\pi^3} P(\alpha\beta\gamma) Im[P^{\alpha}_{vv'} P^{\beta}_{v'c} P^{\gamma}_{cv}]\left(\frac{1}{\omega^3_{cv}\omega^2_{v'c}} + \frac{2}{\omega^4_{vc}\omega_{cv'}}\right)$$

Here, *α, β, γ* are Cartesian components, and *v/v′, c/c′* denote valence bands and conduction bands. And $P(\alpha\beta\gamma)$, ω_{ij} and P^{α}_{ij} refer to full permutation, the band energy difference and momentum matrix elements, respectively.

In order to more intuitively display the contribution of electronic orbitals to the SHG effect, the SHG-weighted charge density analysis scheme, the contribution to the SHG coefficient of all the occupied and unoccupied bands is determined by a "band-resolved" scheme and the charge density of the bands is summed up by the SHG weighted factor and visualized in the real space. Thus, the orbitals dominantly contributing to the SHG coefficient are highlighted whereas those contributed less are not displayed. The theoretical methods have been applied with success to analyze SHG coefficients of NLO crystals, in previous study.[43, 44]

Results and Discussion

Structure and description

SRBOC crystallizes in the monoclinic crystal system in chiral space group $P2_1$. The crystal data are summarized in Table 1. SRBOC has four unique Rb atoms, one unique Na atom, six unique B atoms, fifteen unique O atoms, one unique C atom and four hydrogen atoms in the asymmetric unit. There are two formula units per cell. The fundamental building blocks (FBBs) of SRBOC are $[B_6O_9(OH)_3]^{3-}$ and HCO_3^- groups. The former is comprised of three BO_3 groups and three BO_4 groups. Its shorthand notation can be expressed as 6:[(3Δ + 3T)] based on Christ and Clark[45, 46] (Figure 1). Each BO_4 group connects with adjacent two BO_4 groups by sharing common vertex O atoms, forming an infinite chain along the *b*-axis (Figure 1b and Figure S3 in SI). The chirality of the compound could be attributable to this chain arrangement of the chiral BO_4 groups. BO_3 groups bridge the contiguous BO_4 groups with two common O atoms. To the best of our knowledge, this type of $[B_6O_9(OH)_3]^{3-}$ group is a new anionic structural motif in borates. The isolated HCO_3^- groups are located in the cavity of the infinite chains and connected by hydrogen bonding. It is observed that the bond length of C(1)-O(14) is 1.350 Å, which is slightly larger than that of C(1)-O(10) (1.258(3)Å) and C(1)-O(9) (1.266(3)Å) due to the introduction of hydrogen (H(14)) on the O(14).

Table 1. Crystal data and structure refinement for SRBOC.

Empirical formula	$NaRb_3B_6CO_{15}H_4$
Formula weight	600.30
Temperature/K	100.12
Crystal system	monoclinic
Space group	$P2_1$
a/Å	8.988(3)
b/Å	8.889(2)
c/Å	10.068(4)
α/°	90
β/°	114.6(4)
γ/°	90
Volume/Å^3	731.36(5)
Z	2
ρ_{calc}g/cm^3	2.726
μ/mm^{-1}	10.106
F(000)	564.0
Crystal size/mm^3	0.112 × 0.068 × 0.044
Radiation	MoKα (λ = 0.71073)
2θ range for data collection/°	4.45 to 66.322
Index ranges	$-13 \leq h \leq 13$, $-13 \leq k \leq 13$, $-15 \leq l \leq 15$
Reflections collected	15255
Independent reflections	5011 [R_{int} = 0.0416, R_{sigma} = 0.0519]
Goodness-of-fit on F^2	1.029
Final R indexes [I>=2σ (I)]	R_1 = 0.0306, wR_2 = 0.0570
Final R indexes [all data]	R_1 = 0.0391, wR_2 = 0.0589
Largest diff. peak/hole / e·Å^{-3}	0.82/-0.83
Flack parameter	0.010 (5)

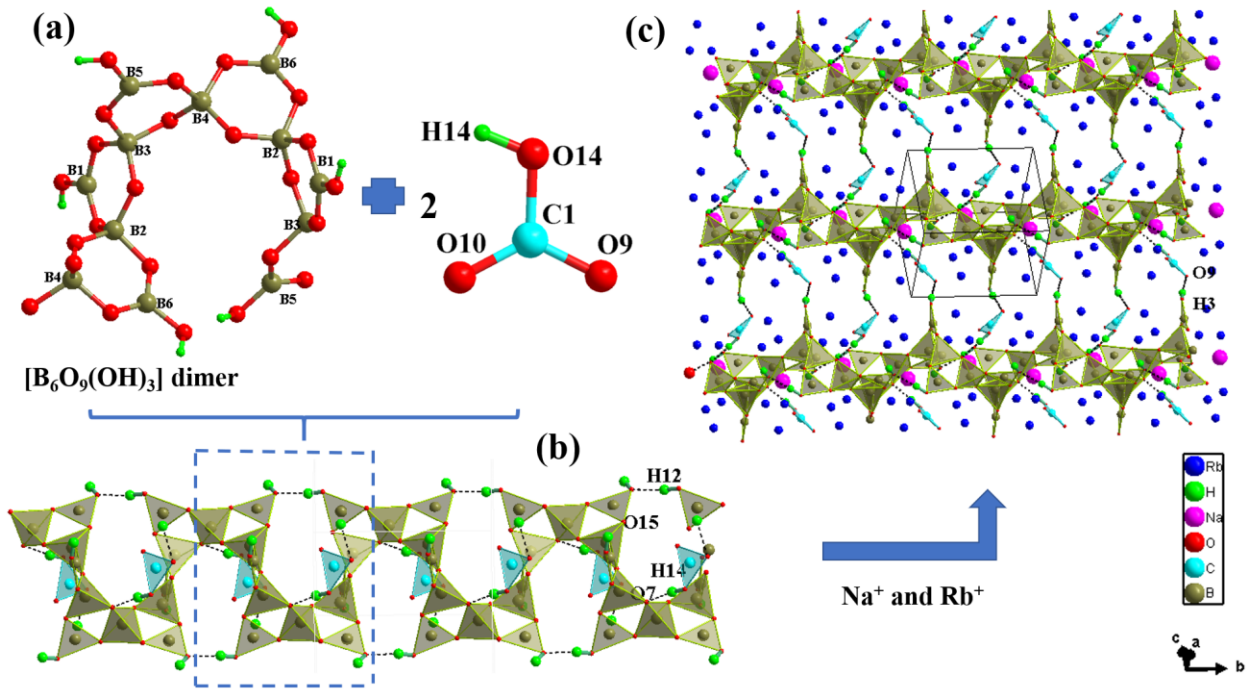

Figure 1. The structure of SRBOC, (a) the $[B_6O_9(O)_3]$ dimer and HCO_3^- group; (b) $[B_6O_9(OH)_3(HCO_3)]_\infty$ chain along *b*-axis, (c) polyhedral representation and projection of the structure of SRBOC (the Rb-O bonds and Na-O bonds are removed for clarity).

Both Rb^+ and Na^+ cations provide compensating positive charges in the structure and are located between adjacent boron-oxygen chains (Figure 1c). The Na^+ cations are six coordinated whereas the Rb^+ cations are eight or nine coordinated. The Na-O bonds length range from 2.354(12) Å to 2.649(7) Å while Rb-O bonds length vary from 2.766(1) Å to 3.590(8) Å. The incorporation of different kinds of cations in different sites in structures requires that their interactions with neighbouring anions should be understood. It is interesting to find that Na^+ cations only bond to those oxygen atoms belonged to the non-hydroxyl group, whereas the Rb^+ cations bond to two kinds of oxygen atoms, non-hydroxyl group oxygen and hydroxyl group oxygen, (see Figure 2). The exact reason for these bonding characters is unclear. However, given the different size of the Na^+ and Rb^+ cations, of which the ionic radii are 1.12 Å in seven-coordination and 1.63 Å in nine-coordination respectively,[47] it is important to contain cations with different size to fill different cavities and stabilize the crystal structure.

In addition, there are three kinds of hydrogen bonding in the structure. The first kind occurs between the H(14) atoms in the HCO_3^- groups and the O(8) atoms in the chain with

distance of 1.751(5) Å. The second one exists between O(9) in the HCO_3^- group and H(3) atoms in the chain OH^- groups with distance of 1.954(2) Å. The last type of hydrogen bonding connects H(15) atoms and O(12) atoms in the chain with the length of 1.994(3) Å. Bond valence calculations,[48] Rb 1.09-1.23; Na 1.15; B 3.02-3.04; C 3.94; O 1.83-2.11 are consistent with oxidation states of +1, +1, +3 and +4 for Rb, Na, B, C, and non-hydroxyl O, respectively. In addition, reasonable bond valence sums (BVS) of 1.00-1.13 for Rb and 0.99 for Na were also obtained with applying the updated R_0 values by F.A. Rabuffetti.[49] The calculated BVS for O(12), O(14) and O(15) are -1.17, -1.30 and -1.20 respectively, suggesting these are OH^- groups. The assignment of OH groups was also confirmed by the IR data.

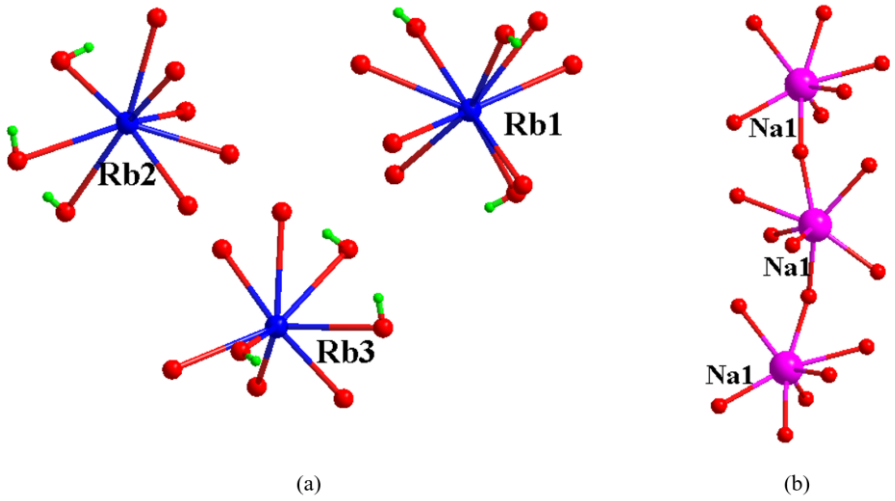

Figure 2. The coordination environments of (a) the Rb^+ and (b) Na^+ cations.

IR Spectroscopy

In order to further confirm the coordination environments of anionic groups in the structure, IR spectroscopic measurements were carried out (see Figure 3). The broad absorption band around 3549 cm^{-1} and 3415 cm^{-1} is assigned to the asymmetric and symmetric vibrations of O-H bonds respectively. The bands in the range of 1430 - 1333 cm^{-1} can be assigned to the B-O and C-O asymmetrical stretching of the BO_3 and CO_3 units, whereas the bands around 1221 cm^{-1}, 1149 cm^{-1} and 1053 cm^{-1} can be assigned to the B-O and C-O stretching vibrations of the BO_4 and CO_3 units. The bands near 965 cm^{-1}, 916 cm^{-1} and 852 cm^{-1} are associated with the symmetric stretching vibrations of the BO_3 and BO_4 units. The bending vibrations of the BO_3

and BO_4 units are found in the range of 796~676 cm^{-1}. These assignments are consistent with the crystal structure, as well as what has been reported in the literature.[26]

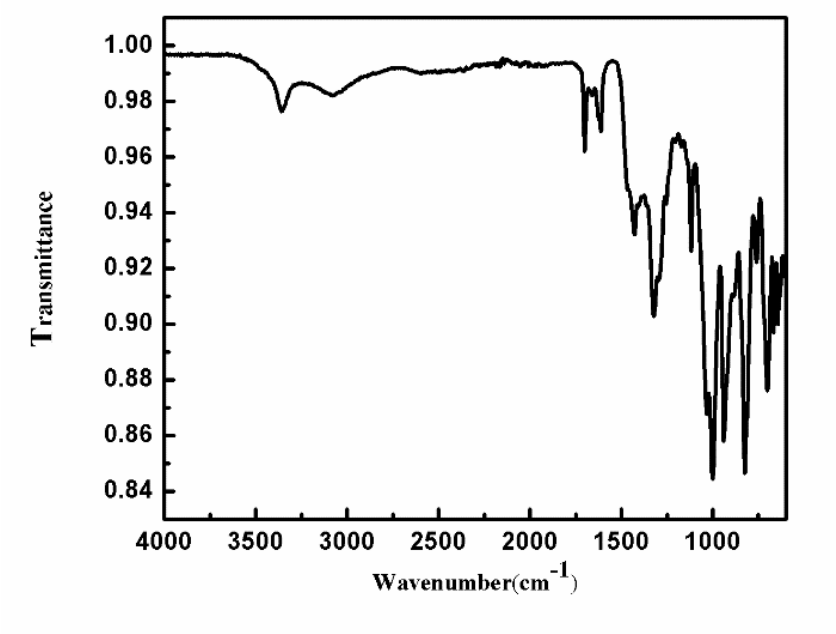

Figure 3. The IR spectrum for SRBOC.

UV−Vis Diffuse Reflectance Spectroscopy

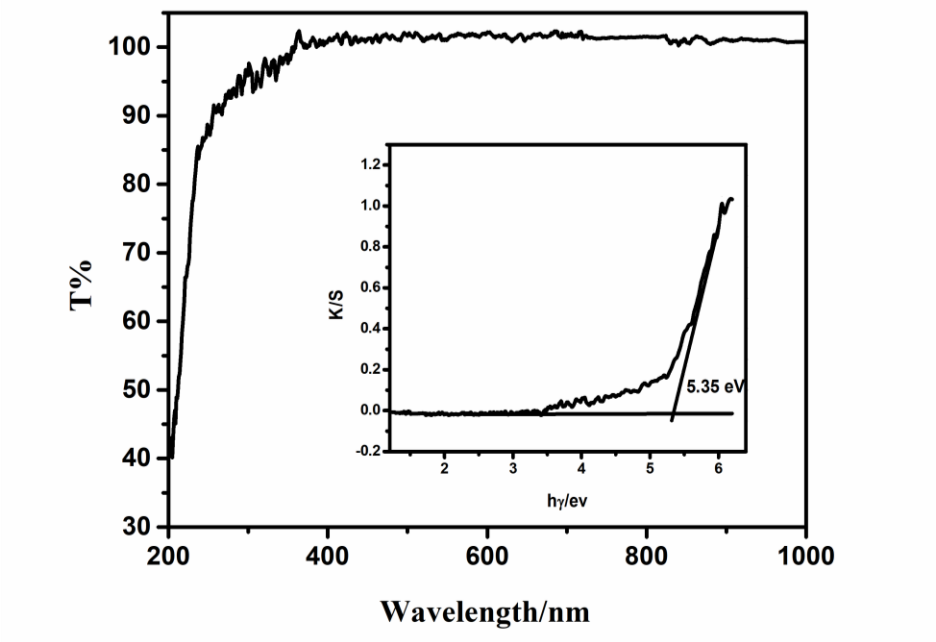

Figure 4. The UV-Vis-NIR diffuse reflectance spectrum for SRBOC.

The UV-Vis-IR diffuse-reflectance spectra between 200-1000 nm for SRBOC is shown in Figure 4. Absorption (*K*/*S*) data were calculated from the following Kubelka–Munk function: $F = (1-R)^2/2R = K/S$, where *R* represents the reflectance, *K* the absorption and *S* the scattering. The minima in the second-derivative curves of the Kubelka–Munk function are taken as the maxima of the absorption bands. The transparency of about 40% at 200 nm indicates SRBOC exhibits wide optical transparent range. The main distribution may be explained by that the dangling oxygen atoms in boron-oxygen building units were removed through B-O and O-H bonds. It is important to increase the energy gap of the anionic group. This kind of structure would be beneficial for a wider transparency range on the UV side.[50]

Thermal Analysis

The compound SRBOC is stable up to about 329 °C even though the compound consists of hydroxyls and HCO_3^- groups (see Figure 5). In comparison, bicarbonate such as sodium bicarbonate and potassium bicarbonate will decompose into corresponding carbonate at around 80 °C and 200 °C, respectively. When SRBOC is heated, the weight loss was 9.0 % over the range from room temperature to 600 °C, that corresponds to the removal of the hydroxyls as the form of water molecules and decomposition of HCO_3^-. The increasing weight in TG curve before 120 °C (~1.01 %) may be due to the absorption of helium gas or error.

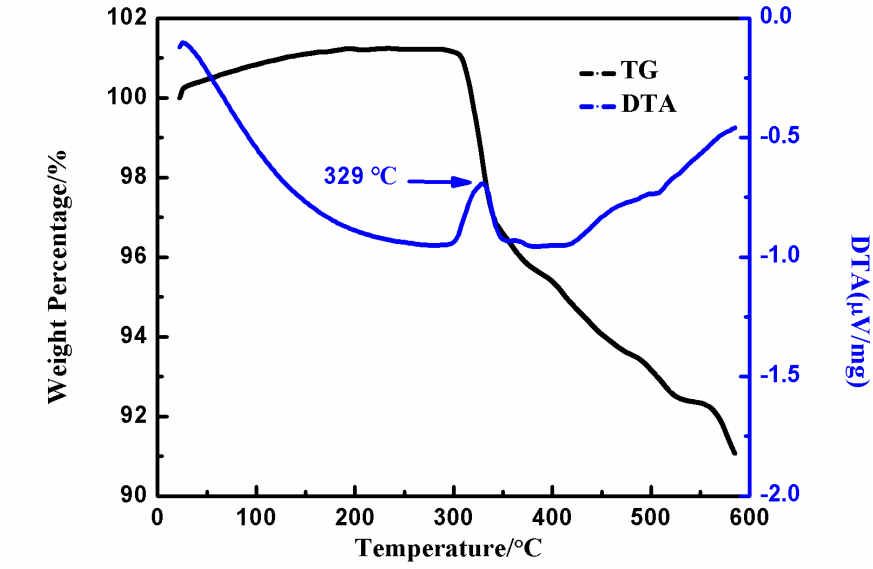

Figure 5. The TG/DTA curves for SRBOC.

Second Harmonic Generation.

The non-centrosymmetric structure of the SRBOC suggests SHG is possible. Powder SHG (PSHG) measurements using a 1064 nm Nd-YAG laser revealed that the SHG intensity of SRBOC is 0.5×SiO_2 in the same particle size range of 90-125 μm (Figure S4 in the SI). From the viewpoint between structure and property, the arrangement of BO_3 and HCO_3^- groups of the compound SRBOC in one cell was shown in Figure 6. For clarity and discussion purpose, the hydrogen atoms are omitted, HCO_3 planes are simplified to CO_3 planes. Following the common practice of considering parallel arrangement of triangular BO_3 or CO_3 planes to be needed to contribute SHG effect, unparallel arrangements were found in the title compound, which might explain the weak SHG effect of SRBOC material. Specifically, the angles of 90.3°, 167.4°, 101.2° and 139.9° were observed between the planes $C(1)O_3$ - $C(1)O_3$, $B(1)O_3$ - $B(1)O_3$, $B(5)O_3$ - $C(1)O_3$ and $B(1)O_3$ - $C(1)O_3$, respectively (Figure 6).

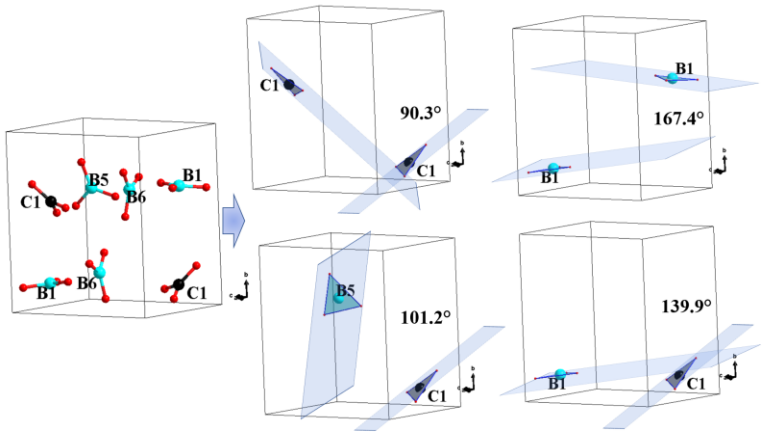

Figure 6. Arrangement of the CO_3 and BO_3 planes in SRBOC.

Theoretical calculation

The calculated band structure (see Figure 7) for $NaRb_3B_6O_9(OH)_3(HCO_3)$ reveals that the compound is an indirect band gap material with the value of 5.01 eV by the PBE functional. Since the electronic transitions from occupied states to unoccupied states reflect the origin of the optical properties, it is necessary to analyze the partial density of states (PDOS) of $NaRb_3B_6O_9(OH)_3(HCO_3)$. The top region of the valence bands is mainly occupied by the 2*p* orbitals of the boron, carbon and oxygen atoms. And a wide hybridization between B/C 2*s*, 2*p* orbitals and O 2*p* orbitals is shown in the range from -10 to 0 eV. In addition, the non-bonding *p*

orbitals of O dominates in region I. As for the bottom region of the conduction bands, it is mainly occupied by the s, *p* states of Na, Rb and *p* states of C, B atoms.

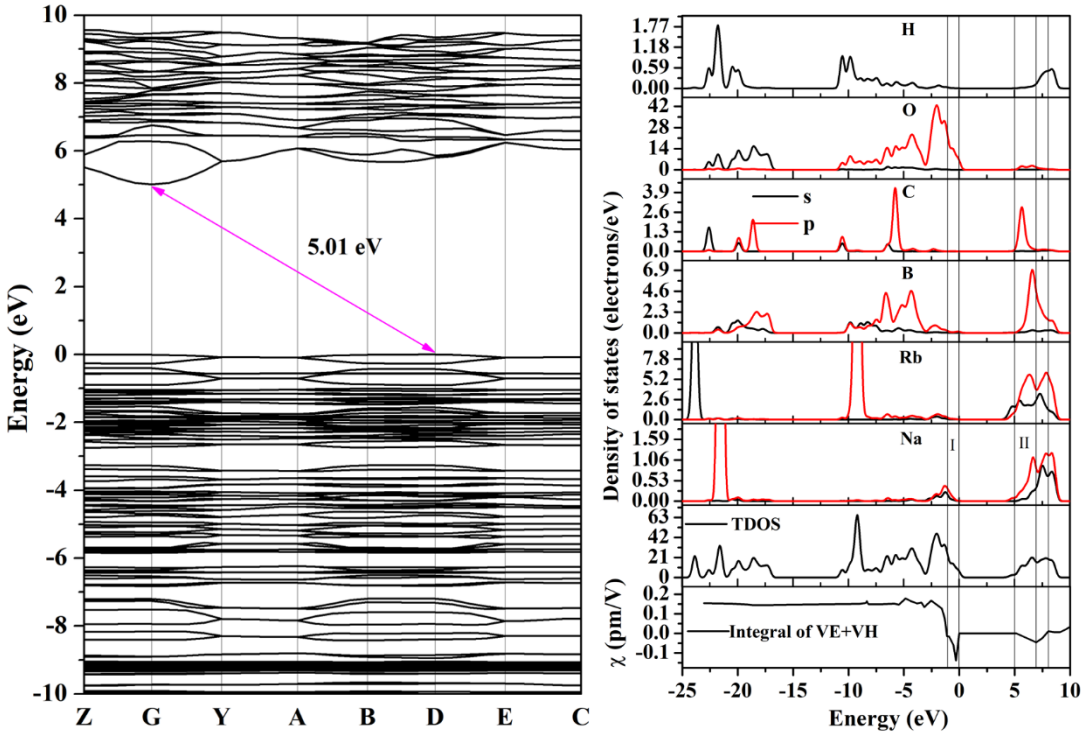

Figure 7. Band structures and PDOS of SRBOC. I-II regions refer to the main contribution region in valence bands, the main contribution region in conduction bands.

The SHG coefficients of this compound were also estimated under the sum-over-states method. The non-vanishing independent SHG tensors are d_{16}= 0.078 pm/V, d_{14} = 0.096 pm/V, d_{22} = 0.198 pm/V and d_{23} = -0.222 pm/V. To demonstrate the contribution of each atom in the SHG processes in the real space, the SHG-density method was used. It should be noticed that the two virtual transition processes, namely virtual electron (VE) and virtual hole (VH) processes, contribute SHG process. From the band-resolved result within the energy band framework which corresponds to individual electronic states of SHG coefficients, the contributions of the VH processes and VE processes are 13.02% and 86.98%. Therefore, VE processes are extremely predominant. SHG densities of VE processes are analyzed. Figure 8 shows the SHG densities of occupied and unoccupied states of $NaRb_3B_6O_9(OH)_3(HCO_3)_2$. It clearly shows that the O atoms play an important role in the occupied states. The B and O atoms make major contributions to the unoccupied states. Besides, HCO_3^- groups make some contributions to SHG both in the occupied

and unoccupied states. The SHG density indicates that the B-O groups (especially BO_3) have main contribution to SHG effect, and the secondary contribution is from HCO_3^- groups.

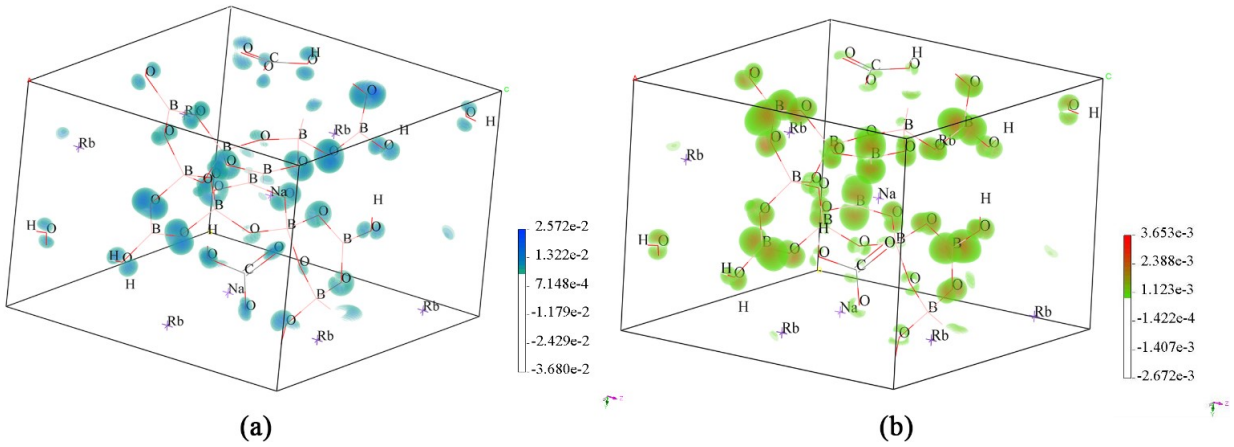

Figure 8. SHG-density of occupied (a) and unoccupied (b) states in SRBOC.

Comparing the properties of molecular HCO_3^-, CO_3^{2-}, and BO_3^{3-} groups.

Atomic-level structural changes can lead to a large difference of SHG effect. For example, the optical properties of HCY-based compounds differed significantly from those based on H_2CY ($C_3N_3O_3^{3-}$, CY)[10, 51] The scarcity of NLO material compounds containing HCO_3^- group promotes us to evaluate the polarizability anisotropy and first order hyperpolarizability of the HCO_3^- group. As we know, an optical polarizability anisotropy (δ) contributes directly to the electric birefringence while the first order hyperpolarizability ($|\beta_{max}|$) contributes to molecular dc electric field-induced second harmonic generation. These values of CO_3^{2-} and BO_3^{3-} groups were obtained as well to compare. The results are in Figure 9. The similar values of δ and $|\beta_{max}|$ for CO_3^{2-} and BO_3^{3-} groups were found due to their similar structure and bond property. However, with the introduction of hydrogen into a CO_3^{2-} group, the $|\beta_{max}|$ value of the resulting HCO_3^- group is much larger (about four times) than that of CO_3^{2-} group, which will benefit larger SHG effect if a proper arrangement of the HCO_3^- groups can be obtained. In SRBOC, even though HCO_3^- possesses higher hyperpolarizability, the arrangement and the density of each building unit in the compound must also be considered in determining their individual contributions to the SHG effect of the material.

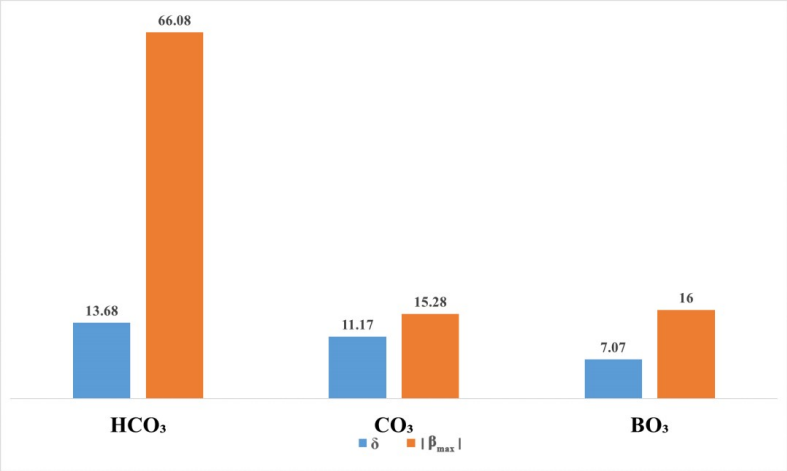

Figure 9. Calculated polarizability anisotropy (δ) and hyperpolarizability (|βmax|) of the HCO_3^-, CO_3^{2-} and BO_3^{3-} groups.

Conclusions

A new non-centrosymmetric borate-bicarbonate, $NaRb_3B_6O_9(OH)_3(HCO_3)$, was synthesized by facile solvothermal method, and its crystallographic parameters and structure were defined. The titled compound presents a new type of chain structure with the $[B_6O_9(OH)_3]^{3-}$ and HCO_3^- groups as basic building units. Transmittance spectroscopy data indicate that this compound has a wide transmission range from 200 to 1200 nm. The compound could be thermally stable up to ~320 °C. The discovery of the compound enriches the structural chemistry of borates and carbonates. The calculated hyperpolarizability ($|\beta_{max}|$) of the HCO_3^- group is much larger than that of CO_3^{2-} and BO_3^{3-} groups, which means a possibility in relatively higher SHG effect if a proper arrangement of the HCO_3^- group can be obtained, such as parallel pattern. We hope that these approaches applied here can be useful to design and discover other new optically active crystals.

Conflicts of interest

The authors declare no competing financial interest.

ASSOCIATED CONTENT

Supporting Information

X-ray crystallographic file in CIF format and experimental and calculated XRD patterns;

Accession Codes

CCDC 1842851 contains the supplementary crystallographic data for this paper. These data can be obtained free of charge via www.ccdc.cam.ac.uk/data_request/cif, or by emailing data_request@ccdc.cam.ac.uk, or by contacting The Cambridge Crystallographic Data Centre, 12 Union Road, Cambridge CB2 1EZ, UK; fax: +44 1223 336033.

Acknowledgements

This work was supported by funding from the National Science Foundation (Awards DMR-1904701). The single crystal X-ray data and FT-IR measurements were acquired at Northwestern University′s Integrated Molecular Structure Education and Research Center (IMSERC) at Northwestern University which is supported by grants from NSF-NSEC, NSF-MRSEC, the KECK Foundation, the State of Illinois, and Northwestern University. This work made use of the J. B. Cohen X-Ray Diffraction Facility supported by the MRSEC program of the National Science Foundation (DMR-1720139) at the Materials Research Center of Northwestern University. WG and PSH thank the Welch Foundation (Grant E-1457) for support.

AUTHOR INFORMATION

Corresponding Author

* Email: krp@northwestern.edu.

Author Contributions

The manuscript was written through contributions of all authors. All authors have given approval to the final version of the manuscript.

References

1. Halasyamani, P. S.; Poeppelmeier, K. R., Noncentrosymmetric Oxides. *Chem. Mater.* **1998**, *10*, 2753-2769.

2. Tran, T. T.; Yu, H.; Rondinelli, J. M.; Poeppelmeier, K. R.; Halasyamani, P. S., Deep Ultraviolet Nonlinear Optical Materials. *Chem. Mater.* **2016**, *28*, 5238-5258.

3. Dewey Jr, C.; Cook Jr, W.; Hodgson, R.; Wynne, J., Frequency doubling in $KB_5O_8{\cdot}4H_2O$ and $NH_4B_5O_8{\cdot}4H_2O$ to 217.3 nm. *Appl. Phys. Lett.* **1975**, *26*, 714-716.

4. Umemura, N.; Kato, K., Phase-matched UV generation at 0.1774 μm in $KB_5O_8 \cdot 4H_2O$. *Appl. Opt.* **1996**, *35*, 5332-5335.

5. Zacharias, H.; Anders, A.; Halpern, J.; Welge, K., Frequency doubling and tuning with $KB_5O_8 \cdot 4H_2O$ and application to NO ($A^2\Sigma+$) excitation. *Opt. Commun.* **1976**, *19*, 116-119.

6. Chen, C.; Wang, G.; Wang, X.; Xu, Z., Deep-UV nonlinear optical crystal $KBe_2BO_3F_2$-discovery, growth, optical properties and applications. *Appl. Phys. B.* **2009**, *97*, 9-25.

7. Zhou, Y.; Wang, G.; Li, C.; Peng, Q.; Cui, D.; Xu, Z.; Chen, C., Sixth harmonic of a Nd: YVO_4 laser generation in KBBF for ARPES. *Chin. Phys. Lett.* **2008**, *25*, 963.

8. Wang, G.; Wang, X.; Zhou, Y.; Li, C.; Zhu, Y.; Xu, Z.; Chen, C., High-efficiency frequency conversion in deep ultraviolet with a $KBe_2BO_3F_2$ prism-coupled device. *Appl. Opt.* **2008**, *47*, 486-488.

9. Lu, J.; Yue, J.; Xiong, L.; Zhang, W.; Chen, L.; Wu, L., Uniform alignment of non-π-conjugated species enhances deep ultraviolet optical nonlinearity. *J. Am. Chem. Soc.* **2019**, *141*，8093-8097.

10. Lu, J.; Lian, Y.; Xiong, L.; Wu, Q.; Zhao, M.; Shi, K.; Chen, L.; Wu, L., How to maximize birefringence and nonlinearity of π-conjugated cyanurates. *J. Am. Chem. Soc.* **2019**, *141*, 16151-16159.

11. Luo, M.; Liang, F.; Song, Y.; Zhao, D.; Xu, F.; Ye, N.; Lin, Z. S., $M_2B_{10}O_{14}F_6$ (M = Ca, Sr): Two Noncentrosymmetric Alkaline Earth Fluorooxoborates as Promising Next-Generation Deep-Ultraviolet Nonlinear Optical Materials. *J. Am. Chem. Soc.* **2018**, *140*, 3884-3887.

12. Yu, H.; Young, J.; Wu, H.; Zhang, W.; Rondinelli, J. M.; Halasyamani, P. S., The Next-Generation of Nonlinear Optical Materials: $Rb_3Ba_3Li_2Al_4B_6O_{20}F$—Synthesis, Characterization, and Crystal Growth. *Adv. Opt. Mater.* **2017**, *5*, 1700840-1700847.

13. Wu, H.; Yu, H.; Pan, S.; Halasyamani, P. S., Deep-Ultraviolet Nonlinear-Optical Material $K_3Sr_3Li_2Al_4B_6O_{20}F$: Addressing the Structural Instability Problem in $KBe_2BO_3F_2$. *Inorg. Chem.* **2017**, *56*, 8755-8758.

14. Zhao, S.; Kang, L.; Shen, Y.; Wang, X.; Asghar, M. A.; Lin, Z.; Xu, Y.; Zeng, S.; Hong, M.; Luo, J., Designing a Beryllium-Free Deep-Ultraviolet Nonlinear Optical Material without a Structural Instability Problem. *J. Am. Chem. Soc.* **2016**, *138*, 2961-2964.

15. Zhao, S.; Gong, P.; Luo, S.; Liu, S.; Li, L.; Asghar, M. A.; Khan, T.; Hong, M.; Lin, Z.; Luo, J., Beryllium-free $Rb_3Al_3B_3O_{10}F$ with reinforced interlayer bonding as a deep-ultraviolet nonlinear optical crystal. *J. Am. Chem. Soc.* **2015**, *137*, 2207-2210.

16. Wu, H.; Yu, H.; Yang, Z.; Hou, X.; Su, X.; Pan, S.; Poeppelmeier, K. R.; Rondinelli, J. M., Designing a deep-ultraviolet nonlinear optical material with a large second harmonic generation response. *J. Am. Chem. Soc.* **2013**, *135*, 4215-4218.

17. Luo, M.; Liang, F.; Song, Y.; Zhao, D.; Ye, N.; Lin, Z., Rational Design of the First Lead/Tin Fluorooxoborates $MB_2O_3F_2$ (M = Pb, Sn), Containing Flexible Two-Dimensional $[B_6O_{12}F_6]$infinity Single Layers with Widely Divergent Second Harmonic Generation Effects. *J. Am. Chem. Soc.* **2018**, *140*, 6814-6817.

18. Zhang, B.; Shi, G.; Yang, Z.; Zhang, F.; Pan, S., Fluorooxoborates: Beryllium-Free Deep-Ultraviolet Nonlinear Optical Materials without Layered Growth. *Angew. Chem. Int. Ed.* **2017**, *56*, 3916-3919.

19. Shi, G.; Wang, Y.; Zhang, F.; Zhang, B.; Yang, Z.; Hou, X.; Pan, S.; Poeppelmeier, K. R., Finding the Next Deep-Ultraviolet Nonlinear Optical Material: $NH_4B_4O_6F$. *J. Am. Chem. Soc.* **2017**, *139*, 10645-10648.

20. Wang, X.; Wang, Y.; Zhang, B.; Zhang, F.; Yang, Z.; Pan, S., CsB_4O_6F: A Congruent-Melting Deep-Ultraviolet Nonlinear Optical Material by Combining Superior Functional Units. *Angew. Chem. Int. Ed.* **2017**, *56*, 14119–14123.

21. Tran, T. T.; Young, J. S.; Rondinelli, J. M.; Halasyamani, P. S., Mixed-Metal Carbonate Fluorides as Deep-Ultraviolet Nonlinear Optical Materials. *J. Am. Chem. Soc.* **2017**, *139*, 1285-1295.

22. Tran, T. T.; He, J.; Rondinelli, J. M.; Halasyamani, P. S., $RbMgCO_3F$: A New Beryllium-Free Deep-Ultraviolet Nonlinear Optical Material. *J. Am. Chem. Soc.* **2015**, *137*, 10504-10507.

23. Zou, G.; Ye, N.; Huang, L.; Lin, X., Alkaline-alkaline earth fluoride carbonate crystals $ABCO_3F$ (A= K, Rb, Cs; B= Ca, Sr, Ba) as nonlinear optical materials. *J. Am. Chem. Soc.* **2011**, *133*, 20001-20007.

24. Kang, L.; Luo, S.; Huang, H.; Ye, N.; Lin, Z.; Qin, J.; Chen, C., Prospects for Fluoride Carbonate Nonlinear Optical Crystals in the UV and Deep-UV Regions. *J. Phys. Chem. C* **2013**, *117*, 25684-25692.

25. Luo, M.; Ye, N.; Zou, G.; Lin, C.; Cheng, W., $Na_8Lu_2(CO_3)_6F_2$ and $Na_3Lu(CO_3)_2F_2$: rare earth fluoride carbonates as deep-UV nonlinear optical materials. *Chem. Mater.* **2013**, *25*, 3147-3153.

26. Liu, L.; Yang, Y.; Huang, J.; Dong, X.; Yang, Z.; Pan, S., Design and Syntheses of a Series of Novel Mixed Borate and Carbonate Halides. *Chem.: Eur. J.* **2017**, *23*, 1521-3765.

27. Liao, C.; Wen, Y.; Lii, K., High-Temperature, High-Pressure Hydrothermal Synthesis of $Ba_3[B_6O_{10}(OH)_2](CO_3)$ and $Ba_6[B_{12}O_{21}(OH)_2](CO_3)_2$, Two Barium Borate Carbonates with 2D Layer and 3D Framework Structures. *Inorg. Chem.* **2018**, *57*, 11492-11497.

28. Abudoureheman, M.; Wang, L.; Zhang, X.; Yu, H.; Yang, Z.; Lei, C.; Han, J.; Pan, S., $Pb_7O(OH)_3(CO_3)_3(BO_3)$: first mixed borate and carbonate nonlinear optical material exhibiting large second-harmonic generation response. *Inorg. Chem.* **2015**, *54*, 4138-42.

29. Zhao, J.; Li, R., $Ba_2(BO_3)_{1-x}(CO_3)_xCl_{1+x}$: A Mixed Borate and Carbonate Chloride Crystallized from High-Temperature Solution. *Inorg. Chem.* **2012**, *51*, 4568-4571.

30. Zhang, X.; Wu, H.; Cheng, S.; Han, G.; Yang, Z.; Pan, S., $K_9[B_4O_5(OH)_4]_3(CO_3)X{\cdot}7H_2O$ (X= Cl, Br): Syntheses, Characterizations, and Theoretical Studies of Noncentrosymmetric Halogen Borate–Carbonates with Short UV Cutoff Edges. *Inorg. Chem.* **2019**, *58*, 106974-6982.

31. Kubelka, P.; Munk, F., An article on optics of paint layers. *Z. Tech. Phys.* **1931**, *12*, 593-601.

32. Tauc, J., Absorption edge and internal electric fields in amorphous semiconductors. *Mater. Res. Bull.* **1970**, *5*, 721-729.

33. CrysAlis PR. Agilent Technologies Ltd. Yarnton, Oxfordshire, England. **2014**.

34. Dolomanov, O. V.; Bourhis, L. J.; Gildea, R. J.; Howard, J. A.; Puschmann, H., OLEX2: a complete structure solution, refinement and analysis program. *J. Appl. Crystallogr.* **2009**, *42*, 339-341.

35. Spek, A. L., Single-crystal structure validation with the program PLATON. *J. Appl. Crystallogr.* **2003**, *36*, 7-13.

36. Sham, L. J.; Schlüter, M., Density-functional theory of the energy gap. *Phys. Rev. Lett.* **1983**, *51*, 1888-1891.

37. Clark, S. J.; Segall, M. D.; Pickard, C. J.; Hasnip, P. J.; Probert, M. I. J.; Refson, K.; Payne, M. C., First principles methods using CASTEP. *Z. Kristallogr.* **2005**, *220*, 567-570.

38. Perdew, J. P.; Burke, K.; Ernzerhof, M., Generalized gradient approximation made simple. *Phys. Rev. Lett.* **1996**, *77*, 3865-3868.

39. Rappe, A. M.; Rabe, K. M.; Kaxiras, E.; Joannopoulos, J. D., Optimized pseudopotentials. *Phys. Rev. B.* **1990**, *41*, 1227-1230.

40. Aversa, C.; Sipe, J. E., Nonlinear optical susceptibilities of semiconductors: rewults with a length-gauge analysis. *Phys. Rev. B.* **1995**, *52*, 14636-14645.

41. Zhang, B.; Lee, M.; Yang, Z.; Jing, Q.; Pan, S.; Zhang, M.; Wu, H. P.; Su, X.; Li, C. S., Simulated pressure-induced blue-shift of phase-matching region and nonlinear optical mechanism for $K_3B_6O_{10}X$ (X = Cl, Br). *Appl. Phys. Lett.* **2015**, *106*, 031906-031911.

42. Lin, J.; Lee, M.; Liu, Z.; Chen, C., Mechanism for linear and nonlinear optical effects in β-BaB_2O_4 crystals. *Phys. Rev. B.* **1999**, *60*, 13380-13389.

43. Lei, B.; Yang, Z.; Yu, H.; Cao C.; Li, Z.; Hu, C.; Poeppelmeier, K. R.; Pan, S. L., A module-guided design scheme for deep-ultraviolet nonlinear optical materials, *J. Am. Chem. Soc.* **2018**, *140*, 10726-10733.

44. Su, X.; Yang, Z.; Lee, M.; Pan, S.; Wang, Y.; Fan, X.; Huang, Z.; Zhang, B., Evidence of "new hot spots" from determining the nonlinear optical behavior of materials: mechanism studies on vanadium borate crystal $Na_3VO_2B_6O_{11}$. *Phys. Chem. Chem. Phys.* **2015**, *17*, 5338-5344.

45. Christ, C.; Clark, J. R., A crystal-chemical classification of borate structures with emphasis on hydrated borates. *Phys. Chem. Miner.* **1977**, *2*, 59-87.

46. Heller, G., A survey of structural types of borates and polyborates. In *Structural Chemistry of Boron and Silicon*, Springer: 1986; pp 39-98.

47. Chen, C.; Lin, Z.; Wang, Z., The development of new borate-based UV nonlinear optical crystals. *Appl. Phys. B* **2005,** *80*, 1-25.

48. Brese, N.; O'keeffe, M. Bond-valence parameters for solids. *Acta Crystallogr. B* **1991**, *47*, 192-197.

49. Yee, T. A.; Suescun, L.; Rabuffetti, F. A., Bond valence parameters for alkali–and alkaline-earth–oxygen pairs: derivation and application to metal− organic compounds. *J. Solid State Chem.* **2019**, *270*, 242-246.

50. Xia, M.; Li, R., Structure and optical properties of a noncentrosymmetric borate $RbSr_4(BO_3)_3$. *J. Solid State Chem.* **2013**, *197*, 366-369.

51. Lin, D.; Luo, M.; Lin, C.; Xu, F.; Ye, N., KLi $(HC_3N_3O_3)\cdot 2H_2O$: Solvent-drop Grinding Method toward the Hydro-isocyanurate Nonlinear Optical Crystal. *J. Am. Chem. Soc.* **2019,** *141*, 3390-3394.

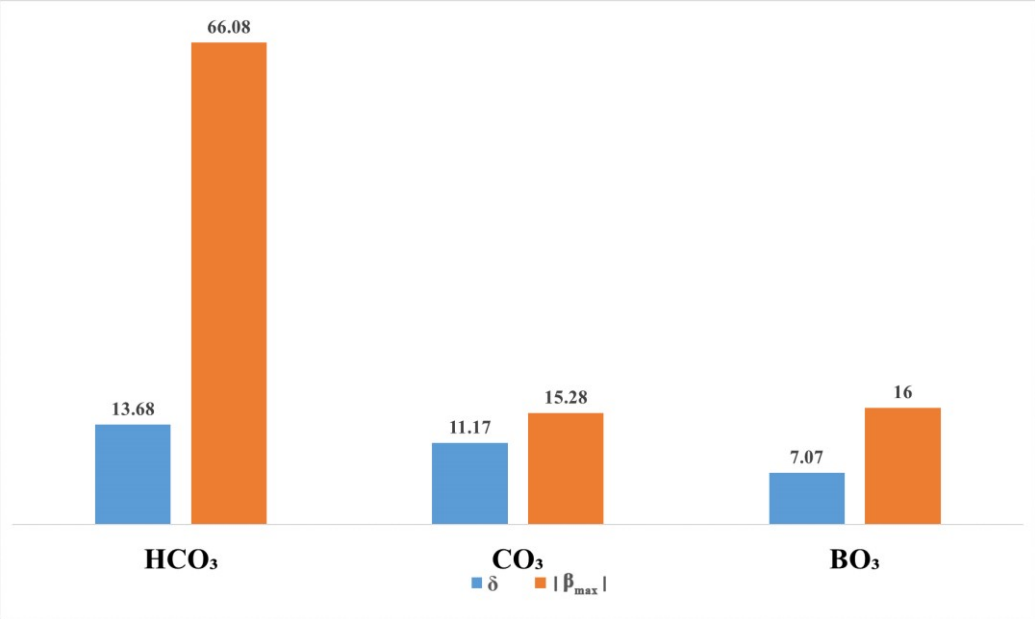

Table of Contents graphic

Synopsis: A new non-centrosymmetric compound, $NaRb_3B_6O_9(OH)_3(HCO_3)$, was obtained by a solvothermal method. It represents the first borate-bicarbonate example. We discuss the crystal structure and calculate the optical properties of the compound. The bicarbonate (HCO_3^-) anion is found to have enhanced hyperpolarizability relative to the carbonate (CO_3^{2-}) anion according to theoretical calculation. In addition, the crystal growth, optical properties, and thermal stability of compound are reported.